Available online at www.sciencedirect.com

ScienceDirect

Procedia Structural Integrity 80 (2026) 392–402

Structural Integrity Procedia

www.elsevier.com/locate/procedia

Fracture, Damage and Structural Health Monitoring

# Investigation of J-integral in Hydrogen-promoting environment

L.Gritti[a]*, D. Fiorona[a], S. Ferrari[a], M. Pelucchi[a], M. Cabrini[a], T. Pastore[a]

[a] *University of Bergamo, Dalmine (BG), 24044, Italy*

**Abstract**

The conversion of existing natural gas pipelines into hydrogen transport systems is crucial for the sustainable energy transition. To assess the impact of hydrogen-promoting environments on mechanical behavior, it is essential to conduct in-situ testing where hydrogen charging and mechanical testing are performed concurrently. Hydrogen can form on the surface of pipeline metals through dissociation from the gas phase or electrochemical reduction of hydrogen ions via cathodic protection or over protection. Once atomic hydrogen enters the material, it can diffuse rapidly through the metal lattice, accumulating at critical concentrations and leading to "hydrogen damage". The steels used in gas pipelines are immune to hydrogen embrittlement (HE), however HE phenomena can occur under conditions of slow plastic deformation, often due to soil movement. Therefore, it is necessary to perform hydrogen charging in conjunction with mechanical tests, such as elastic-plastic mechanical testing to simulate these conditions. This study investigates the mechanical behavior of API 5L grade X65 pipeline steel. An experimental setup was developed to conduct elastic-plastic fracture mechanics tests on SE(B) samples while concurrently performing electrochemical hydrogen charging. The hydrogen charging was carried out in an alkaline solution, simulating the presence of water in soils. Tests were conducted in both air and hydrogen environments, and the effects of hydrogen embrittlement were analyzed using the J-integral approach.



*Keywords:* Mechanical fracture tests, Cathodic protection, J-integral in environment, Hydrogen embrittlement, Pipeline steel

* Corresponding author. Tel.: +39 035 205 2052.
*E-mail address:* luca.gritti1@unibg.it


10.1016/j.prostr.2026.02.037

## 1. Introduction

Ensuring the compatibility between metallic materials dedicated to natural gas transportation and hydrogen-promoting environment is crucial today to conquer the energy transition. Recent studies have been conducted by various authors on this topic. Sofian et al., (2024) and Zhao et al., (2024) investigated the compatibility of hydrogen, both in its pure form and when mixed with other gases. Additionally, Meng et al., (2017); Peral et al., (2024); and Hamed et al., (2025) analyzed the susceptibility of metal alloys to hydrogen embrittlement.

To assess the impact of hydrogen-promoting environments on mechanical behavior, it is essential to conduct in-situ testing where hydrogen charging and mechanical testing are performed concurrently. Hydrogen charging can be carried out using two approaches. Using gaseous hydrogen charging, which requires a complex experimental setup and poses safety risks because of the high hydrogen pressures that must be reached. Via electrochemical charging with cathodic polarization, this second experimental set-up is easily to control, and it is more efficient to charge the hydrogen, as demonstrated by Koren et al., (2023); and Hoschke et al., (2025). The cathodic polarization develop hydrogen on the surface of the sample by reduction reaction. Following chemisorption mechanism, the molecular hydrogen can dissociate in the atomic and penetrate in the material. However, the hydrogen embrittlement phenomena can be observed only if the presence of hydrogen is associated with slow plastic deformation as demonstrated by Cabrini *et al.*, (2020). This condition is typically present on pipeline and caused by soil movement as describe by Niazi *et al.*, (2021). To simulate this condition the slow strain rate tests (SSR) or elastic-plastic mechanical fracture tests (EPMF) must be adopted. However, during SSR tests, cracks due to hydrogen embrittlement are only observed after the specimen has reached necking, and therefore, they occur only in a relatively short section of the test. The EPMF tests are employed for elastic-plastic materials, primarily focusing on the evaluation of the J parameter. This parameter quantifies the energy required to propagate a defect. Specifically, the J-integral-based resistance curve is utilized to characterize a ductile material's resistance to crack initiation, stable crack growth, and the onset of tearing instability.

Thus, to achieve the in-situ electrochemical hydrogen charging concurrently on the plastic deformation due to mechanical tests, the EPMF with single edge specimen (SE(B)) oriented upside down compared to the conventional configuration are used. It is possible to monitor the crack opened mouth via clip gauge executing the mechanical test with immersed sample. During cathodic charging the hydrogen can reach the crack tip through two primary mechanisms: by recalling hydrogen that is already dispersed within the material or through external input. Both mechanisms create a hydrogen-rich area around the crack, exacerbating the problem. The first mechanism involves diffusive hydrogen, which can migrate through the metal lattice and accumulate in areas with lower hydrogen concentration. The creation of new surfaces due to crack propagation alters the lattice structure and promotes the formation of hydrogen-poor areas, which can attract more hydrogen from the specimen. In these conditions the atomic hydrogen tends to concentrate around the most stressed area (around the defect) as indicated by Cabrini *et al.*, (2015) reducing the material's toughness.

In this work, a system was developed to perform simultaneous elastic-plastic fracture mechanics testing and cathodic charging in an alkaline solution. It was investigated the mechanical behavior of API 5L grade X65 pipeline steel. The tests were conducted in air and compared with those performed with environment presences. The effects of electrochemical hydrogen charging, maintained throughout the execution of the test, were analyzed and compared via J-integral curves and fracture surfaces analysis.

## 2. Experimental

### *2.1. Materials and Solutions*

The test was performed on Single Edge Bend SE(B) specimens of high-strength low-alloy (HSLA) API 5L-grade X65 steel, obtained from a 24’’diameter, 14 mm thick hot-rolled, longitudinally welded pipe for gas and oil transport, with a ferritic–pearlitic banded microstructure. The chemical composition of steel is reported in Table 1.

Table 1:Composition of material HSLA X65 grade

| Elem. | C | Mn | Si | P | S | Nb | Mo | V | Cu | Ni | Cr | $C_{eq}$ |
|---|---|---|---|---|---|---|---|---|---|---|---|---|
| [%WT] | 0.09 | 1.64 | 0.24 | 0.003 | 0.002 | 0.049 | 0.002 | <0.0000 | 0.011 | 0.017 | 0.031 | 0.366 |

The specimens were designed following the ASTM 1820 as shown in Figure 1. “C-L” crack plane identification was used, as reported by ASTM E399. The crack plane propagation was parallel to the longitudinal axes of pipe to simulate the longitudinal propagation of defects. The specimen’s dimensions, given in Table 2, were 8 mm thickness (B) and 24 mm wide (W), the W/B ratio equal to 3 was adopted. The support span was 96 mm. The W/B ratio is not optimal, although it complies with regulatory requirements, due to the constraints imposed by the pipe geometry. The specimens were produced by machining while the integrated knives for applying the double-cantilever Clip-In Displacement gage (COD) and chevron notch were produced via Electrical Discharge Machining (wire EDM). Both specimen sides were polished up to 1200 grit and degreased in acetone. The M4 thread was made in the thickness of the specimen (away from specimen’s holders) for connecting the working pin during electrochemical charging.

About the test in environment, an alkaline solution was considered: a 26.5 g/l of $Na_2CO_3$ + 42 g/l of $NaHCO_3$ carbonate–bicarbonate solution of pH 10, adopted by Parkins and Zhou, (1997) to simulate soil water in studies on stress corrosion cracking. It was adopted the -1.05 V vs SCE polarization to simulate the cathodic protection applied on pipeline network.

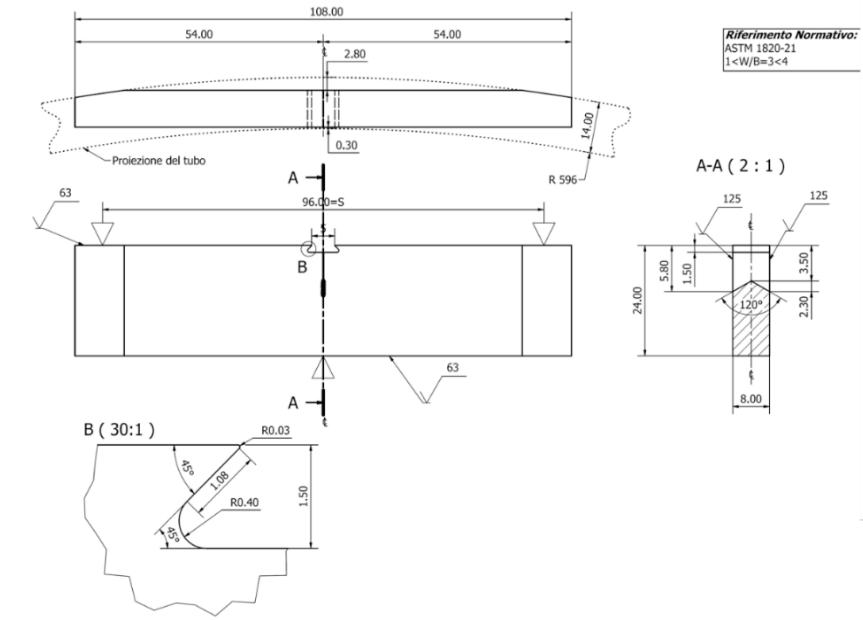


Figure 1: Specimen dimension

Table 2: Dimension of SE(B) specimen

| Specimen thickness B [mm] | Width W [mm] | Support Span S [mm] | Notch Depth [mm] |
|---|---|---|---|
| 8 | 24 | 96 | 7.70 |

### 2.2. Experimental Lay-Out

The three-point bend apparatus was produced to measure the fracture toughness of the SE(B) specimens in air and in situ cathodically hydrogen charging. Experimental setup consists of a polymethyl methacrylate electrochemical cell positioned above the oil-hydraulic traction machine as shown in Figure 2. The specimen, acting as the working electrode, is oriented upside down compared to the conventional configuration. This arrangement allows for the attachment of the clip gauge (COD measure) while keeping the specimen fully submerged throughout the entire test, thereby ensuring the maintenance of cathodic polarization. The cell was equipped with a calomel reference electrode positioned near to the crack surface and activated titanium counter electrode.

### 2.3. Experimental Procedure

The experimental procedure consists of double steps: fatigue pre-cracking procedure and mechanical fracture toughness test.

The purpose of fatigue pre-cracking procedure was made a trigger defect to promote progress the crack during the mechanical fracture toughness test simulating a natural crack. To obtain the reproducibility of pre-cracking it was adopted decreasing ΔK approach imposing the parameter resumed in Table 3. It was imposed the notch depth as initial crack size, the final crack length equal to 10.8 mm (it was standard minimum value acceptable estimating as 0.45 W) and the final K value equal 14 Mpa·√m. These conditions guarantee the sufficient smaller residual load and little plastic radius in the final crack tip. The pre-cracking configuration involves in load control configuration, producing by cyclically loading at ratio R=0.1 executed at 8 Hz in sinusoidal waveform to guarantee good machine feedback. The compliance was monitored. When the value of experimental compliance estimating as ratio of COD over force was reached, the target value was imposed the next load step.

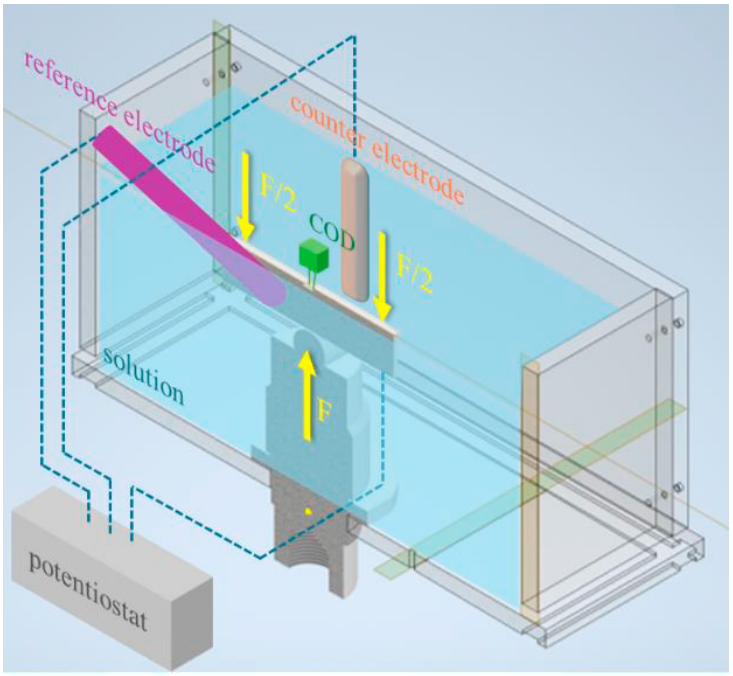


Figure 2: Experimental Lay-Out

Table 3: Pre-cracking parameters

| Step | K | $a_{final}$ | $a_{initial}$ | f(a/W) | $P_{max}$ | $P_{min}$ | ΔP | $C_{LL}$ target | $r_p$ |
|---|---|---|---|---|---|---|---|---|---|
| [-] | [Mpa √m] | [mm] | [mm] | [-] | [kN] | [kN] | [kN] | [mm/N] | [mm] |
| 1 | 27.34375 | 9.5 | **7.7** | 1.393076 | 4.6264 | 0.4626 | 4.1638 | 4.06E-06 | 0.575 |
| 2 | 21.875 | 10 | 9.5 | 1.45617 | 3.5408 | 0.3541 | 3.1867 | 4.48E-06 | 0.368 |
| 3 | 17.5 | 10.4 | 10 | 1.511065 | 2.7297 | 0.2730 | 2.4568 | 4.87E-06 | 0.235 |
| 4 | **14** | **10.8** | 10.4 | 1.570464 | 2.1012 | 0.2101 | 1.8911 | 5.31E-06 | 0.151 |

The mechanical fracture toughness tests involved a procedure directed toward evaluation of complete fracture toughness resistance curve using an elastic unloading procedure as described by ASTM 1820 (procedure 2). The tests were performed in displacement mode, with a displacement of 80 μm applied during the loading phase, followed by a 30 μm displacement during the unloading phase, as controlled by the clip gauge. This approach ensured continuous traction on the sample throughout both phases. The displacement velocity was maintained at a constant rate of $3 \cdot 10^{-5}$ mm/s. Multiple cycles were conducted for each test, with the test interruption determined based on the experimental curve obtained during each cycle. The same parameters of mechanical tests were adopted also to mechanical tests within situ hydrogen charging. The sample was submerged in solution and connected at the potentiostat. It was applied the cathodic protection during all mechanical tests.

After the test was completed, the specimens were opened in liquid nitrogen to identify the ending of mechanical test and measuring correctly the crack lengths on samples surface. The sample tested under cathodic protection was pickled in inhibited hydrochloric acid to remove the oxidize products without damaging the fracture surface.

## 3. Theory and Calculations

The J-integral curve represents the strain energy release rate, thus the energy absorbed per unit fracture surface area during crack propagation. Rice, (1968) defined energy J as a path-independent line integral that characterizes near-crack tip stresses and strains under elastic and/or elastoplastic material behaviors. Therefore, from the integral of load/displacement experimental curve, it was possible to estimate the sufficient energy to promote a crack propagation.

### *3.1. Estimation of J-Δa curve*

The calculation procedure involved estimating each cycle (loading, unloading) of load $P_{(i)}$, defined as the last point before unloading, and the crack length $a_{(i)}$, based on the unloading branch (characterized by linear elastic behavior). The crack length was estimated by compliance $C_{LL(i)}$, defined by relation (1).

$$C_{LL(i)} = \frac{\Delta v_i}{\Delta P_i}$$

$$a_{(i)} = 0.999748 - 3.9504\,u + 2.9821\,u^2 - 3.21408\,u^3 + 51.51564\,u^4 - 113.031\,u^5$$

$$u = \frac{1}{\sqrt{\frac{\left(B - \frac{(B - B_N)^2}{B}\right) W\, E\, C_{LL(i)}}{\frac{S}{4}}} + 1} \tag{1}$$

The plane-strain fracture toughness $K_{(i)}$ was estimate at force $P_{(i)}$ as follows

$$K_i = \frac{P_i S}{\sqrt{B\, B_N}\, W^{\frac{3}{2}}} \cdot f\left(\frac{a_i}{W}\right)$$

$$f\left(\frac{a_i}{W}\right) = \frac{3\left(\frac{a_i}{W}\right)^{\frac{1}{2}}\left[1.99 - \left(\frac{a_i}{W}\right)\left(1 - \frac{a_i}{W}\right)\left(2.15 - 3.93\left(\frac{a_i}{W}\right) + 2.7\left(\frac{a_i}{W}\right)^2\right)\right]}{2\left(1 + 2\frac{a_i}{W}\right)\left(1 - \frac{a_i}{W}\right)^{\frac{3}{2}}} \tag{2}$$

It was calculated $J_{(i)}$ for each cycle as sum of elastic and plastic contribution (equation (3))

$$J_{(i)} = J_{el(i)} + J_{pl(i)} \tag{3}$$

Defining the elastic component as follows

$$J_{el(i)} = \frac{(K_i)^2 \cdot (1 - \nu^2)}{E}$$

And plastic component as follows

$$J_{pl(i)} = \left[J_{pl(i-1)} + \left(\frac{\eta_{pl(i-1)}}{b_{i-1}}\right) \cdot \frac{A_{pl(i)} - A_{pl(i-1)}}{B_N}\right] \cdot \left[1 - \gamma_{i-1} \cdot \left(\frac{a_i \cdot a_{i-1}}{b_{i-1}}\right)\right]$$

Where $A_{pl(i)}$ was defined in equation (4) as the increment of plastic area under the chosen force versus plastic displacement record between lines of constant plastic displacement between two cycles.

$$\begin{gathered} A_{pl(i)} = A_{pl(i-1)} + \frac{[P_i + P_{i-1}] \cdot [V_{pl(i)} - V_{pl(i-1)}]}{2} \\ b_{i-1} = [W - a_{i-1}] \\ \eta_{pl} = 2 + 0.522\,\frac{b_{i-1}}{W} \\ \gamma_{i-1} = 1.0 + \frac{0.76 \cdot b_{i-1}}{W} \end{gathered} \tag{4}$$

Thus, it was possible estimate the $J_{(i)} - \Delta a_{(i)}$ curve at first attempt. The standard suggests fitting the data to correct the value of first estimation on initial crack length $a_0$ solving the system in equation (5). Thus, it was estimated the new $K_{(i)}$ and new $J_{(i)}$ as shown in the equations (2) (3).

$$\begin{Bmatrix} \sum a_i - \frac{\sum J_i}{2\,\sigma_Y} \\ \sum a_i J_i^2 - \frac{\sum J_i^3}{2\,\sigma_Y} \\ \sum a_i J_i^3 - \frac{\sum J_i^4}{2\,\sigma_Y} \end{Bmatrix} = \begin{bmatrix} n & \sum J_i^2 & \sum J_i^3 \\ \sum J_i^2 & \sum J_i^4 & \sum J_i^5 \\ \sum J_i^3 & \sum J_i^5 & \sum J_i^6 \end{bmatrix} \cdot \begin{Bmatrix} a_{0\,adj} \\ B \\ C \end{Bmatrix} \tag{5}$$

### *3.2. Estimation $J_Q$ values and validation of data*

To estimate the critical initiation $J_Q$, a construction line was defined to establish the fitting area for validating the results, as outlined in the ASTM 1820 standard. The $J_Q$ was then estimated by the intersection between the J-curve and

the construction line at a displacement of 0.2 mm. Therefore, the values were checked to establish the correctness of the analysis, in particular:

- $|a_{0q} - a_0| < 0.01W$ or $|a_{0q} - a_0| < 0.5\ mm$
- Number of considered points in the fitting $N°_{p.ti\ calcolo\ a_{0q}} > 8$
- Number of points in the region $0.4\,J_Q \div J_Q \geq 3$
- Constant of the fitting $C_2 < 1$

To validate the value of $J_Q$ as the critical $J_{Ic}$ and estimate the values of $K_{Jic}$, the standard provides post-validation checks that correlate the obtained results with thickness and ligament, as detailed below:

$$B > 10\frac{J_Q}{\sigma_Y}$$

$$b_0 > 10\frac{J_Q}{\sigma_Y}$$

with $\sigma_Y = \frac{\sigma_{YS}+\sigma_{UTS}}{2}$

In conclusion it was possible to estimate the $K_{Jic}$,

$$K_{J_{Ic}} = \sqrt{E' J_{Ic}} = \sqrt{\frac{E}{1-\nu^2} \cdot J_{Ic}}$$

## 4. Results and discussion

All samples show the comparable fatigue pre-crack length as optically measured in Figure 3 and reported in Table 4 using the weighted average method as specified by the standard. The minimum pre-cracking length is 0.45 W equal to 10.8 mm. However, the pre-cracking value was underestimated in order to have a larger ligament available during the mechanical test. This is due to the small sample size imposed by the dimensions of the tube from which they were extracted. The discrepancy between the crack propagation optically measured ($\Delta a_{opt}$) and that determined using prediction compliance method ($\Delta a_{pred}$) should not exceed the 0.15 mm of $\Delta a_{pred}$. The air test satisfies this condition, whereas the test conducted under cathodic polarization does not. This is due to the inhomogeneous propagation front, especially in the test conducted in environment. As a result, it was difficult to estimate the crack lengths. However,

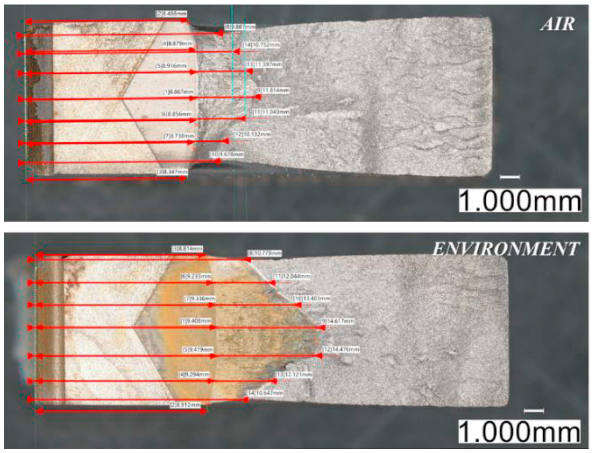


Figure 3: Crack length measurements following fatigue pre-cracking and at the conclusion of the mechanical test after opening in liquid nitrogen for test conducted in air and environment under cathodic polarization (not pickled)

distinct behavioral effects can still be observed. A significant necking is present on the specimen tested in air, while it is much less pronounced on the specimen tested under cathodic protection. This suggests that the presence of hydrogen caused less lateral contraction (deformation) in the specimen tested under cathodic protection.

Table 4: Measures of crack length after test in Air and Environment of SE(B) samples

| N° | AIR | | ENVIRONMENT | |
|---|---|---|---|---|
| | **$a_{pre\text{-}cracking}$** [mm] | **$a_{end\ of\ mechanical\ test}$** [mm] | **$a_{pre\text{-}cracking}$** [mm] | **$a_{end\ of\ mechanical\ test}$** [mm] |
| $a_1$ | 8.488 | 9.887 | 8.814 | 10.779 |
| $a_2$ | 8.879 | 10.752 | 9.233 | 12.044 |
| $a_3$ | 8.916 | 11.397 | 9.336 | 13.403 |
| $a_4$ | 8.867 | 11.814 | 9.408 | 14.617 |
| $a_5$ | 8.856 | 11.04 | 9.419 | 14.479 |
| $a_6$ | 8.738 | 10.132 | 9.294 | 12.121 |
| $a_7$ | 8.347 | 9.678 | 8.912 | 10.647 |
| $a_{mean}$ | **8.779** | **10.820** | **9.259** | **12.896** |
| $\Delta a_{optical\ meas.}$ | **2.040** | | **3.637** | |
| $\Delta a_{predicted}$ | 2.070 | | 2.601 | |
| $\lvert\Delta a_{opt}-\Delta a_{pred}\rvert<0.15\ \Delta a_{pred}$ | 0.030<0.311→pass | | 1.036<0.385 →not pass | |

The experimental results of loading curves, as reported in the Figure 4, indicated a quite difference between the test conducted in air (AIR) and in environment under cathodic polarization (ENV), after reaching the maximum load (B zone in the graph). The curves begin at ≈2 kN because the tests must start above pre-cracking residual load. These branches of load/unload are similar because the elastic behavior is predominant in respect to the plastic and depends on geometry of the sample that is equal (A zone in the graph). However, the ENV test started to decrease after reaching the maximum load while in the AIR test the force increasing continuously and remains approximately constant during opening of mouth of sample, except for the formation of a plastic hinge. Thus, at the same COD a lower force was measured in ENV instead of air test. This part of curve is affected mostly by plastic behavior. This difference it was imputed at cathodic hydrogen supply. Thus, the presence of hydrogen leads to embrittlement phenomena when reaching the predominant plastic behavior of the sample, as confirmed by Fukunaga, (2024).

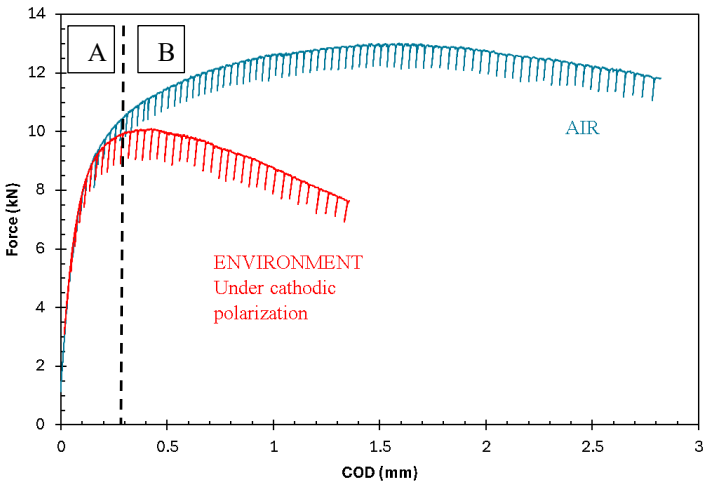


Figure 4: Experimental curves of mechanical test of SE(B) in air and in environment (electrochemical

The J-integral curves, elaborated by experimental data, confirm the hydrogen embrittlement effect on the environment test (Figure 5). The J-curve performed in air shows much more energy to propagate the defect than the one performed in the environment. In fact, during the air test the energy absorbed, thus the work provided during the test, is very high compared with environment tests. Therefore, the material acts more fragile, and the crack propagates at lower energy level provided. These results are confirmed by analysis of fracture surface in Figure 6. The air test denoted a typical ductile fracture characterized by dimples in different sizes and high surface deformation. The small and uniform dimples are present also in the valleys of huge plastic deformed zones denoted to plasticity behavior. Therefore, more energy (work) had to be done to deform the material and propagate the crack. The presence of hydrogen charging from the environment involves in a surface associated with a brittle aspect. The almost total absence of dimples, the presence of semi-cleavage facets, and the secondary cracks along perpendicular plane to principal propagation direction, are typical for hydrogen embrittlement phenomena. The fracture is affected by poor plastic deformation and crack propagate plane cleavage facets. The propagation crack required less energy to take place as confirmed by J-curve.

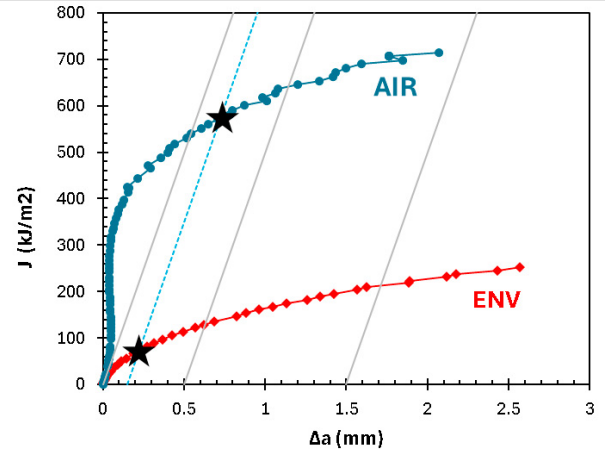


Figure 5: J-integral Curves

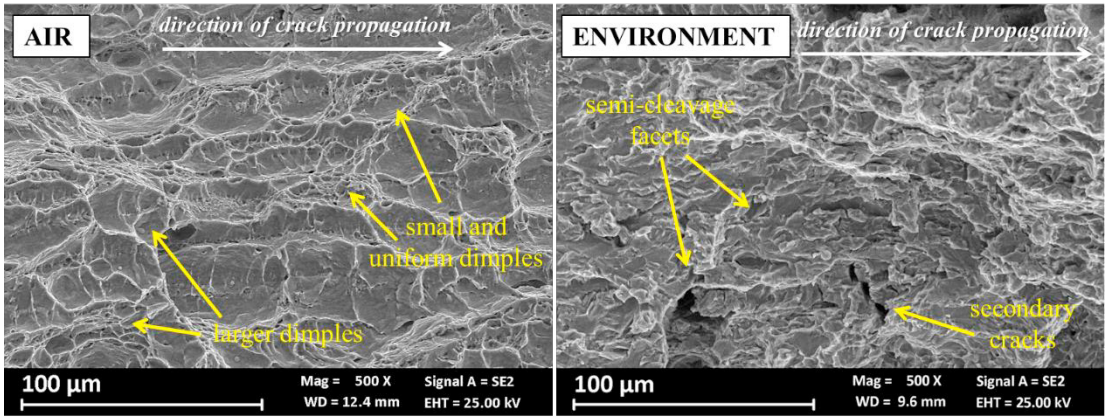


Figure 6: Comparison of fracture surfaces of tests conducted in Air and Environment under cathodic polarization in carbonate-bicarbonate solution (pickled surface)

It was estimating the critical trigger energy to promote the propagation of the defect, reported in Figure 5 (black stars). Thes values indicates the $J_Q$ parameter identified as intersection between J-curve and dashed construction line, the results are compared in the Table 5. Although the $J_Q$ values are not verified as $J_{Ic}$, it is nevertheless observed that the initiation value in air is 7 times higher than that estimated in the presence of hydrogen. The stress intensity factor is 2.5 times higher than that in the environment. Thus, the Hydrogen Embrittlement Reduction (HER) estimated respect to the air parameters is equal to 86% and 62% of $J_Q$ and $K_{JQ}$ respectively.

Table 5: $J_Q$ and $K_{JQ}$ parameter estimated by J-integral curves

| Test | $J_Q$ [kJ/m$^2$] | $J_{Ic}$ [kJ/m$^2$] | HER($J_Q$) [%] | $K_{JQ}$ [Mpa √m] | HER ($K_{JQ}$) [%] |
|---|---|---|---|---|---|
| Air | 587 | not valid | - | 366 | - |
| Carbonates-Bicarbonates under cathodic polarization at -1.05 V vs SCE | 85 | not valid | 85 | 139 | 62 |

## 5. Conclusion

- The experimental system developed permits us to execute elastic-plastic mechanical tests concurrently with hydrogen cathodic charging.
- The pre-cracking procedure results in reproducible fatigue crack lengths.
- The air test exhibits different behavior compared to the electrochemical hydrogen charging test after reaching the maximum load in the load-COD curves.
- The test conducted in environment under cathodic polarization (electrochemical hydrogen charging) showed a much flatter J-integral curve compared to the air exposure test. This indicates that the presence of hydrogen promotes embrittlement at the crack tip, requiring less energy (work) to propagate the defect.
- Fractographic analysis confirms a typical ductile morphology for the air test, with dimples and plastic deformations. The fracture surface of the hydrogen-exposed specimen shows signs of embrittlement, with facets resembling quasi-cleavage.
- The $J_Q$ value in air is 587 kJ/m$^2$, compared to the estimated value of 85 kJ/m$^2$ in the presence of hydrogen, confirming a significant 85% reduction in the energy required to initiate crack propagation.

## References

Cabrini, M. *et al.* ((2015)) 'Environmentally assisted cracking and hydrogen diffusion in traditional and high-strength pipeline steels', *Corrosion Reviews*, 33(6), pp. 529–545. Available at: https://doi.org/10.1515/corrrev-2015-0051.

Cabrini, M. *et al.* ((2020)) 'Hydrogen permeation in X65 steel under cyclic loading', *Materials*, 13(10). Available at: https://doi.org/10.3390/ma13102309.

Fukunaga, A. ((2024)) 'Hydrogen embrittlement behaviors during SSRT tests in gaseous hydrogen for cold-worked type 316 austenitic stainless steel and iron-based superalloy A286 used in hydrogen refueling station', *Engineering Failure Analysis*, 160. Available at: https://doi.org/10.1016/j.engfailanal.2024.108158.

Hamed, A. *et al.* ((2025)) 'Assessing the hydrogen embrittlement susceptibility of an existing L360NB natural gas pipeline steel for 100 % hydrogen transport', *Corrosion Science*, 244. Available at: https://doi.org/10.1016/j.corsci.2024.112648.

Hoschke, J. *et al.* ((2025)) 'Determination of the hydrogen fugacity during cathodic hydrogen charging of X65 D pipeline steel', *Corrosion Science*, 243. Available at: https://doi.org/10.1016/j.corsci.2024.112580.

Koren, E. *et al.* ((2023)) 'Experimental comparison of gaseous and electrochemical hydrogen charging in X65 pipeline steel using the permeation technique', *Corrosion Science*, 215(February). Available at: https://doi.org/10.1016/j.corsci.2023.111025.

Meng, B. *et al.* ((2017)) 'Hydrogen effects on X80 pipeline steel in high-pressure natural gas/hydrogen mixtures', *International Journal of Hydrogen Energy*, 42(11), pp. 7404–7412. Available at: https://doi.org/10.1016/j.ijhydene.2016.05.145.

Niazi, H. *et al.* ((2021)) 'High pH stress corrosion cracking initiation and crack evolution in buried steel pipelines: A review', *Engineering Failure Analysis*. Elsevier Ltd. Available at: https://doi.org/10.1016/j.engfailanal.2020.105013.

Parkins, R.N. and Zhou, S. ((1997)) 'The stress corrosion cracking of C-Mn steel in CO2-HCO3 −CO32 − solutions. II: Electrochemical and other data', *Corrosion Science*, 39(1), pp. 175–191. Available at: https://doi.org/https://doi.org/10.1016/S0010-938X(97)89248-7
.
Peral, L.B. *et al.* ((2024)) 'Effect of electrochemical charging on the hydrogen embrittlement susceptibility of a low-alloyed tempered martensitic steel submitted to high internal pressure', *International Journal of Hydrogen Energy*, 63, pp. 657–667. Available at: https://doi.org/10.1016/j.ijhydene.2024.03.034.

Rice, J.R. ((1968)) *A Path Independent Integral and the Approximate Analysis of Strain Concentration by Notches and Cracks*. Available at: http://asmedigitalcollection.asme.org/appliedmechanics/article-pdf/35/2/379/5449160/379_1.pdf.

Sofian, M. *et al.* ((2024)) 'A review on hydrogen blending in gas network: Insight into safety, corrosion, embrittlement, coatings and liners, and bibliometric analysis', *International Journal of Hydrogen Energy*. Elsevier Ltd, pp. 867–889. Available at: https://doi.org/10.1016/j.ijhydene.2024.02.166.

Zhao, W. *et al.* ((2024)) 'Insights into the role of CO in inhibiting hydrogen embrittlement of X80 steel weld at different hydrogen blending ratios', *International Journal of Hydrogen Energy*, 50, pp. 292–302. Available at: https://doi.org/10.1016/j.ijhydene.2023.10.167.